American Mineralogist, Volume 91, pages 850–861, 2006

Cation order and hydrogen bonding of high-pressure phases in the Al_2O_3-SiO_2-H_2O system: An NMR and Raman study

XIANYU XUE,[1,*] MASAMI KANZAKI,[1] HIROSHI FUKUI,[1] EIJI ITO,[1] AND TAKAFUMI HASHIMOTO[2]

[1]Institute for Study of the Earth's Interior, Okayama University, Misasa, Tottori, 682-0193 Japan
[2]Faculty of Science, Kumamoto University, Kurokami 2-36-1, Kumamoto 860-8555 Japan

ABSTRACT

Topaz-OH, phase egg, and δ-AlOOH are hydrous phases in the Al_2O_3-SiO_2-H_2O system that have been found to be stable at successively higher pressures up to those corresponding to the lower mantle, and thus they may be important water reservoirs in the deep mantle. We have applied ^{1}H, ^{29}Si, and ^{27}Al nuclear magnetic resonance (NMR) and Raman spectroscopy to shed new light on the structure of these phases. ^{29}Si and ^{27}Al NMR results clearly revealed that the Si-Al distribution in phase egg is partially disordered. The presence of structural disorder in topaz-OH was also confirmed. ^{1}H NMR and Raman data are both consistent with strong, but asymmetric hydrogen bonding in δ-AlOOH and phase egg, and a range of hydrogen bonding distances in topaz-OH. The observed structural disorder and hydrogen bonding could be responsible for the high upper temperature stability limits (1500~1700 °C) of phase egg and topaz-OH, and are also relevant to the incorporation mechanisms of water in nominally anhydrous stishovite.

Keywords: NMR spectroscopy, topaz, phase egg, δ-AlOOH, Raman spectroscopy, crystal structure, order-disorder

INTRODUCTION

Water is among the most important volatile components that significantly affect phase relations, and physical and thermodynamic properties of minerals. Increasing evidence suggests that water is not only abundant near the Earth's surface and crust, but may also be present in the deep mantle as either hydrous minerals or nominally anhydrous minerals (cf. Prewitt and Parise 2000). In the Al_2O_3-SiO_2-H_2O system, three hydrous phases have been found to be stable at pressures corresponding to the upper to lower mantle and have been suggested to be potentially important water carriers in the subducted slabs. Among them, topaz-OH [$Al_2SiO_4(OH)_2$], the OH end-member of the F-OH topaz solid solution series, has been reported at pressures between 5.5 and 13 GPa and temperatures up to 1500 °C (Wunder et al. 1993; Schmidt 1995; Ono 1999). The initial successful synthesis of this phase had been surprising because natural topaz minerals show only limited substitution of OH for F, and it was once suggested that the OH/(OH + F) content of topaz could not exceed 50% because of the short H-H distance of 1.5 Å (Parise et al. 1980). At pressures between about 11 and 22 GPa, and temperatures up to about 1700 °C, phase egg ($AlSiO_3OH$) has been reported to become the stable phase (Eggleton et al. 1978; Irifune et al. 1995; Schmidt 1995; Schmidt et al. 1998; Ono 1999; Sano et al. 2004). The relatively high upper temperature stability limits for topaz-OH and phase egg suggest that both may be stable not only in the subducted slabs, but also along normal mantle geotherm (cf. Sano et al. 2004). Above 23 GPa, phase egg breaks down to δ-AlOOH + stishovite below 1200 °C, and to corundum + stishovite + fluid above 1200 °C (Sano et al. 2004). δ-AlOOH, a high-pressure polymorph of diaspore (α-AlOOH) and boehmite (γ-AlOOH), has been found to be stable to pressures above 30 GPa at 1000~1200 °C, and thus it may serve as a water reservoir in the cold subducted slabs, transporting water into the lower mantle (Ohtani et al. 2001; Sano et al. 2004). In addition to these hydrous phases, nominally anhydrous stishovite has also been suggested to be a potentially important water reservoir, especially beyond the stability fields of hydrous phases (Pawley et al. 1993; Chung and Kagi 2002; Panero and Stixrude 2004).

The crystal structure of δ-AlOOH was first refined in the space group of $P2_1nm$ from powder X-ray diffraction (XRD) by Suzuki et al. (2000), although the H position was not determined. The framework of oxygen packing is similar to the $CaCl_2$ (distorted rutile) structure, containing columns of edge-sharing AlO_6 octahedra that are joined via corners (Fig. 1a). More recently, Kudoh et al. (2004) refined the structure of a similar phase containing Mg and Si (δ-$[Al_{0.86}Mg_{0.07}Si_{0.07}]OOH$) in space group *Pnn*2 using single-crystal XRD, and identified two H sites from difference-Fourier maps, H1 with a short O-H1···O hydrogen bonding distance of 2.511 Å, and H2 with two longer O-H2···O distances of 2.743 Å. Raman spectrum of δ-AlOOH was first reported by Ohtani et al. (2001) and contains several broad bands between 1500 and 3000 cm^{-1}. This was interpreted by Kudoh et al. (2004) to be related to the existence of two H sites, although as discussed below, this is unlikely to be true. The strong hydrogen bonding in δ-AlOOH has also been the subject of first principles calculations because it may play a critical role in determining the elastic properties at high pressure (Tsuchiya et al. 2002; Panero and Stixrude 2004). In general, hydrogen bonding in minerals also has great effects on many other properties such as the strength, rheological, and electrical properties, and plays an important role in stabilizing hydrous and nominally

* E-mail: xianyu@misasa.okayama-u.ac.jp

0003-004X/06/0506–850$05.00/DOI: 10.2138/am.2006.2064

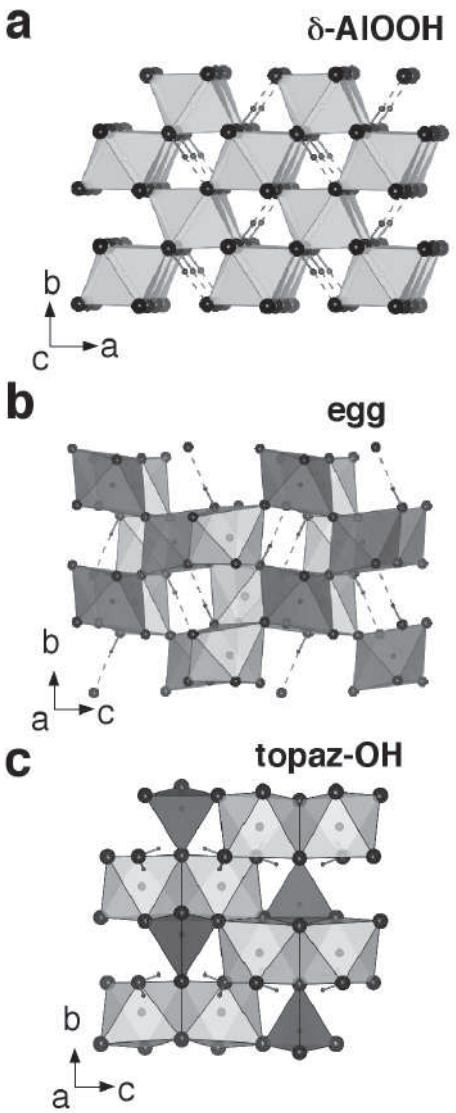

FIGURE 1. (**a**) Crystal structures of δ-AlOOH (Suzuki et al. 2000), (**b**) phase egg (Schmidt et al. 1998), and (**c**) topaz-OH with half-occupancy for the H sites (Northrup et al. 1994). AlO_6 octahedra are light gray, SiO_4 tetrahedra and SiO_6 octahedra are dark gray, large spheres are O atoms, and small spheres are H atoms. Broken lines denote hydrogen bonding with H···O distances <2 Å. The H positions in **a** were obtained from molecular dynamics simulations in this study. Drawings have been produced with VICS-II, developed by K. Momma from the 3D visualization system VENUS (Izumi 2005).

anhydrous phases by lowering the enthalpy, or increasing the entropy, or both (cf. Prewitt and Parise 2000).

The crystal structure of phase egg was determined from powder XRD by Schmidt et al. (1998). The reported structure has a space group $P2_1/n$ and resembles that of stishovite and δ-AlOOH, containing an ordered arrangement of SiO_6 and AlO_6 octahedra linked by both edge- and corner-sharing (Fig. 1b). However, the significance of partial Si-Al disorder was not evaluated in the structural refinement. XRD is known to be intrinsically insensitive to small amounts of such disorder because of the similar scattering factors of Si and Al. Cation disorder is expected to have large effects on the thermodynamic properties and stability fields of minerals (e.g., Navrotsky 1977; Kanzaki et al. 1992). Like δ-AlOOH, phase egg is also characterized by strong hydrogen bonding with an O-H···O distance of 2.577 Å (Schmidt et al. 1998).

The crystal structure of topaz-OH was first refined in space group *Pbnm* from single-crystal XRD by Wunder et al. (1993), although the hydrogen positions could not be located. The reported structure shows close agreement with that of F-rich topaz, containing tetrahedral SiO_4 and linked $AlO_4(OH)_2$ octahedra. These authors also reported infrared (IR) spectrum that contains two OH stretching bands near 3600 and 3520 cm^{-1}, and a pronounced tail toward lower frequency. More recently reported Raman spectrum in the OH stretching region (Komatsu et al. 2005) resembles the IR spectrum. A subsequent single-crystal XRD study (Northrup et al. 1994) reported that the single H position found in F-rich topaz is split into two nonequivalent, half-occupied H positions in topaz-OH (Fig. 1c). They also suggested that the structure is non-centrosymmetric and might have a long-range ordered H distribution with a reduction of symmetry to $Pbn2_1$. A recent lattice energy calculation and molecular dynamics simulation study (Churakov and Wunder 2004) predicted four nonequivalent crystallographic H positions in topaz-OH that are in dynamic exchange at ambient condition and suggested that the instantaneous configuration of H violates all symmetry elements, whereas the space- and time-averaged structure possesses *Pbnm* symmetry.

It is thus clear that although the crystal structures of all three hydrous phases have been determined by XRD, the hydrogen sites and possibility of Si-Al disorder need additional constraints; both factors are expected to critically affect the physical and thermodynamic properties and stability field. In addition, much remains to be learned about the solubility and incorporation mechanisms of water in nominally anhydrous stishovite at very high pressure and temperature (see Ono 1999; Sano et al. 2004). Vibrational spectroscopy (Raman and IR) and ^{1}H MAS NMR are both known to be sensitive probes of hydrogen bonding, with OH stretching frequency showing a positive correlation (cf. Nakamoto et al. 1955; Novak 1974; Libowitzky 1999), and ^{1}H chemical shift showing an inverse correlation (cf. Eckert et al. 1988; Xue and Kanzaki 2004) with hydrogen bonding (O-H···O and H···O) distances. ^{29}Si MAS NMR is particularly useful in providing quantitative information about local structures around Si, and is perhaps the most powerful tool for revealing and quantifying Si-Al disorder because Si with different coordination numbers or different next nearest neighbor (NNN) Si/Al ratios often yield distinct peaks with intensities proportional to site abundances (cf. Kirkpatrick 1988). ^{27}Al MAS NMR can also provide complementary information concerning the coordination and ordering around Al, although peaks are normally broadened and shifted by second-order quadrupolar interaction (cf. Kirkpatrick 1988; Jäger 1994).

We have thus applied Raman and ^{1}H, ^{29}Si, and ^{27}Al NMR spectroscopy to provide additional constraints on the hydrogen bonding and Si-Al disorder in δ-AlOOH, phase egg, and topaz-OH, and on the solubility and incorporation mechanisms of water in nominally anhydrous stishovite. In this paper, we will focus on

δ-AlOOH, phase egg, and topaz-OH. The results for stishovite will be presented in a forthcoming paper, except in cases where the data are useful in the interpretation of spectra collected in this study. We present convincing evidences from ^{29}Si and ^{27}Al NMR for the presence of partial Si-Al disorder in phase egg, and we also show that our data are consistent with local structural disorder, including Si-Al disorder, in topaz-OH. Our ^1H NMR and Raman results both support strong, but asymmetric, hydrogen bonding in δ-AlOOH and phase egg and a range of hydrogen bonding distances in topaz-OH. These results shed new light on the stability fields of these hydrous phases and also have important implications for water incorporation in nominally anhydrous stishovite at very high pressure and temperature.

EXPERIMENTAL METHODS AND SAMPLE DESCRIPTIONS

Sample syntheses and descriptions

The starting material for the syntheses of δ-AlOOH was reagent-grade $Al(OH)_3$ as received. Phase egg and topaz-OH were synthesized from a mixture of dried reagent-grade SiO_2, Al_2O_3, and $Al(OH)_3$ with a nominal bulk composition of $AlSiO_3OH$. For the synthesis of water-bearing aluminous stishovite, a similar starting material with a nominal bulk composition of $0.95SiO_2{\cdot}0.05AlOOH$ was used. Both SiO_2 and Al_2O_3 were dried in a furnace at 1400 °C for 12 h, and the $Al(OH)_3$ was dried in a vacuum oven at 80 °C for 12 h before weighing. The mixture was homogenized by thoroughly grinding in ethyl alcohol and was then dried in a vacuum oven at 80 °C for more than 12 h.

High-pressure sample syntheses have been performed with a 1000 or 5000 ton Kawai-type double-stage uniaxial split-sphere multi-anvil apparatus (USSA-1000 or USSA-5000). Several δ-AlOOH samples have been synthesized at about 21 GPa and 1000 °C for the duration of about 1 h. The starting $Al(OH)_3$ powder was placed directly into a cylindrical Re heater set in a $LaCrO_3$ sleeve for thermal insulation. Phase egg was synthesized at about 17 GPa and 1000 °C for the duration of about 2 h, and topaz-OH was produced at about 12 GPa by maintaining a temperature of 1300 °C for 2 h, followed by heating at 1200 °C for 1 h. Single-phase water-bearing aluminous stishovite was synthesized at about 18 GPa and 1800 °C for the duration of 1 h. The starting mixtures for these experiments were sealed into a Pt capsule by welding to avoid potential water loss. The sample capsule was surrounded by an MgO sleeve inside a cylindrical Re heater, which was in turn insulated by an outer ZrO_2 sleeve. Temperature was measured with W97Re3-W75Re25 thermocouple. The effect of pressure on the EMF of the thermocouple was ignored.

We have characterized the synthesized δ-AlOOH, phase egg, and topaz-OH samples by powder XRD; the latter two phases were also analyzed by the electron microprobe. The recovered δ-AlOOH samples were found to be nearly pure δ-AlOOH phase; the sample for phase egg consists dominantly of fine-grained phase egg (up to about 20 μm) with minor stishovite and corundum; and the sample of topaz-OH consists of large grains (up to about 200 μm) of topaz-OH and kyanite, together with smaller grains (<10 μm) of stishovite. The presence of kyanite in the latter sample may be an indication of water loss. Unit-cell parameters of phase egg were: $a = 7.1475(6)$ Å, $b = 4.3275(3)$ Å, and $c = 6.9472(5)$ Å, $\beta = 98.305(7)°$, in good agreement with those reported by Schmidt et al. (1998). Chemical compositions have been analyzed using a JEOL JXA-8800 electron microprobe at an accelerating voltage of 10 kV, a beam current of 1 nA, and a beam diameter of 2 μm (Table 1). The low beam current was essential to minimize beam damage to the hydrous phases. The average Si/Al atomic ratio is 1.00 (0.03) for phase egg, close to stoichiometry, and 0.43(0.02) for topaz-OH, somewhat lower than expected from stoichiometry. A small amount of Al was also detected in the stishovite phase coexisting with topaz-OH, consistent with previous reports (Pawley et al. 1993; Chung and Kagi 2002; Ono 1999).

TABLE 1. Average electron microprobe analyses

Phase*	Al_2O_3 (wt%)	SiO_2 (wt%)	Total	Si/Al ratio
phase egg sample:				
phase egg(16)	42.0(1.0)	49.5(1.4)	91.5(1.9)	1.00(0.03)
corundum(7)	99.8(1.0)	0.12(0.06)	99.9(1.0)	0.0010(0.0005)
topaz-OH sample:				
topaz-OH(30)	60.4(1.6)	30.7(1.2)	91.1(1.6)	0.43(0.02)
kyanite(13)	62.6(1.1)	38.1(1.3)	100.7(1.4)	0.52(0.02)
stishovite(6)†	2.5(0.4)	100.2(1.0)	102.7(1.0)	34.7(4.7)

* Numbers in parentheses are the numbers of analyses.
† The electron beam volume probably contains surrounding kyanite, because of the small grain sizes (<10 μm) and consistently poor totals.

Raman spectroscopy

We have acquired unpolarized Raman spectra on samples of single crystals or aggregates, using an argon-ion laser with a wavelength of 488 nm and a power of 50 mW in 180° backscattering geometry. The laser beam was focused onto the sample with a 10× objective lens. Light scattered from the sample was focused onto the entrance slit (150 μm width) of a monochromater with a focal length of 500 mm and a grating of 1200 gr/mm, and detected with a liquid nitrogen-cooled CCD detector. Spectra centered near 900, 2400, and 3500 cm^{-1}, with a digital resolution around 1.2 cm^{-1}, have been collected separately. Raman shift was calibrated using the plasma lines of the laser.

We have taken particular precautions to eliminate fluorescence from the environment (light, computer monitor, etc.). To evaluate the presence of fluorescence from the samples and also to check for possible spectral variations that could result from temperature gradient, we have obtained Raman spectra on several grains for each phase across the sample. We found no systematic spectral variations for any of the samples. Some of the grains in the δ-AlOOH samples show visible fluorescence (red color) upon laser irradiation with a pair of strong bands near 877 and 940 cm^{-1}, possibly due to trace impurities of transition metals that might have been introduced during high-pressure synthesis.

^1H, ^{29}Si, and ^{27}Al NMR spectroscopy

We have obtained ^1H, ^{29}Si, and ^{27}Al MAS NMR spectra at a resonance frequency of 400.4, 79.5, and 104.3 MHz, respectively, using a Varian Unity-Inova 400 MHz spectrometer and a Jakobsen-type 5 mm or Doty 4 mm CP-MAS probe. Chemical shifts are referenced externally to tetramethylsilane (TMS) for ^1H and ^{29}Si, and to 1 *M* aqueous solution of $Al(NO_3)_3$ for ^{27}Al.

The ^1H MAS NMR spectra have been obtained with a spectral width of 1 to 2 MHz, a range of sample spinning rates up to 17 kHz, and recycle delay times $>5T_1$ for ^1H (T_1: spin-lattice relaxation time) to ensure full relaxation, except where noted. The ^1H T_1 has been measured with the saturation-recovery method, and was found to be 0.73~2.9 s for the three hydrous phases, but much longer for water-bearing stishovite (see Table 2). The DEPTH sequence, consisting of three back-to-back pulses ($\pi/2 - \pi - \pi$) with a phase cycle of 16 (Cory and Ritchey 1988), has been used to suppress the broad probe background from outside the RF coil. The residual ^1H background signal, which is small for the Jakobsen probe, but moderate for the Doty probe, has been subtracted from the reported spectra by acquiring a spectrum on the same (empty) rotor under identical conditions immediately before each measurement with sample loaded. Spectra acquired using the two probes are identical after background subtraction.

We have collected both single-pulse ^{29}Si MAS NMR and ^1H-^{29}Si cross-polarization (CP)-MAS NMR spectra for phase egg and topaz-OH, but report only the latter because of the poor signal/noise (S/N) ratio of the former. ^1H-^{29}Si CP-MAS NMR is a valuable technique for obtaining ^{29}Si NMR spectra on natural-abundance (4.7% ^{29}Si) high-pressure hydrous samples with limited sizes (e.g., Phillips et al. 1997). The experiment detects the magnetization generated by polarization transfer from ^1H to ^{29}Si during a period of "contact time" when radiofrequency (RF) fields for ^1H and ^{29}Si satisfying the MAS-modified Hartmann-Hahn matching conditions are applied. The variation of signal intensity with contact time can be described by two time constants: T_{SiH} for the rate of cross polarization and $T_{1\rho}(H)$ for ^1H spin-lattice relaxation in the rotating frame. The former is particularly useful, because it has been shown to correlate with the Si-H distances (cf. Phillips et al. 1997). We have obtained the ^1H-^{29}Si CP-MAS NMR spectra with a ramped power of the ^{29}Si channel (with a RF field range of 10 kHz) to reduce the instability of the signal level. The MAS-modified Hartmann-Hahn matching condition was adjusted using a natural pyrophyllite sample. The spinning rate was 4 kHz, contact times were 0.01 to 20 ms, and recycle delays were 1 to 3 s.

We have also obtained single-pulse ^{27}Al MAS NMR spectra on all samples, and ^1H-^{27}Al CP-MAS NMR spectra on the phase egg and topaz-OH samples using the Jakobsen probe. Because of its 5/2-spin, ^{27}Al MAS NMR spectra usually contain a central band dominated by the (1/2, –1/2) central transition (CT) that is broadened and shifted by second-order quadrupolar interaction, and many spinning sidebands due to (m, m – 1) (where m = 3/2, 5/2) satellite transitions (ST). Both of these features are known to carry information about the structurally useful parameters of isotropic chemical shift (δ_i), quadrupolar coupling constant (C_Q), and EFG asym-

TABLE 2. ^{1}H, ^{29}Si, and ^{27}Al NMR results

phase	^{1}H NMR			^{29}Si NMR				^{27}Al NMR		
	δ_t^H (ppm)	FWHM* (ppm)	T_1 (s)	Si site	δ_t^{Si} (ppm)	FWHM (ppm)	population(%)	δ_t^{Al} (ppm)	C_Q (MHz)	η_Q
δ-AlOOH	12.5	5.9	2.9(0.3)					13.4(0.5)	3.35(0.05)	0.88(0.03)
Phase egg	12.0	5.9	0.73(0.04)	Si(E2Si1Al)	−183.4(0.06)	4.21(0.08)	21.1(0.6)	11.2†	3.0†	
				Si(E1Si2Al)	−173.8(0.05)	11.2(0.2)	71.8(1.1)			
				Si(E0Si3Al)	−158.2(0.6)	11.2(1.3)	7.1(1.1)			
Topaz-OH	4.1‡		1.37(0.04)	Si^{IV}	−83.3‡		93.4	10†	4.5†	0.7†
				Si^{VI}	−177		6.6(0.5)			
Stishovite§	9.3	0.5	142(7)							

* At a spinning rate of 12 kHz.
† Mean value for a range of parameters.
‡ Maximum of asymmetric peak.
§ Single phase synthesized at 18 GPa and 1800 °C.

metry parameter (η_Q) (cf. Jäger 1994). We have thus acquired single-pulse ^{27}Al MAS NMR spectra with a large spectral width of 2 MHz and a short pulse width of 0.3~0.5 μs (about 30° tip angle for selective central transition) to observe the entire ST spinning sideband pattern. The recycle delay time was 0.2~1.0 s, and the spinning rate was 12 kHz. These spectra contain a small, narrow peak near 103.8 ppm due to AlN impurity in the silicon nitride rotor, and a smaller broad component near 50 ppm from the probe. The effect of the probe/rotor background on the ST spinning sideband pattern is minor, and that on the central band shape can be effectively removed by a background subtraction similar to above (see details below). A spline correction has been applied to remove the rolling baseline resulting from spectrometer deadtime. Simulations of the central band and ST spinning sideband patterns were performed with the STARS software, taking into consideration the finite spinning rate and probe bandwidth (about ±0.6 MHz). The ^{1}H-^{27}Al CP-MAS NMR spectra have been obtained with contact times of 0.1 to 8 ms and a recycle delay of 3 s. A moderately high spinning rate of 10 kHz and a low RF field strength (~8 kHz) have been used to improve the CP efficiency (cf. Vega 1992). A natural pyrophyllite sample was used for the adjustment of the modified Hartmann-Hahn matching condition. The probe background is negligible for the ^{1}H-^{27}Al CP-MAS NMR spectra, which thus yield a reliable central band shape.

NMR measurements for δ-AlOOH and topaz-OH were carried out on powdered samples, whereas those for phase egg were obtained from the recovered sample block (about 4 mg) without crushing, This was accomplished by packing with dried KBr powder in the rotor. The NMR spectra for the latter, nevertheless, can be treated as powder patterns because of the small grain sizes and lack of preferred orientation. To avoid complications due to contamination, we have handled all samples except δ-AlOOH with clean gloves and tweezers. The samples of δ-AlOOH were powders initially prepared with no special precautions taken for powder XRD measurements, and may have suffered from minor organic contaminations (see below). Although the topaz-OH, and to a minor degree, phase egg samples contain other coexisting phases (stishovite and kyanite or corundum), it is possible, with a judicious choice of recycle delay time, to completely eliminate their contributions to the ^{1}H MAS, and ^{1}H-^{29}Si and ^{1}H-^{27}Al CP-MAS NMR spectra, because kyanite and corundum are essentially anhydrous, and stishovite has low H contents and extremely long ^{1}H T_1. Such experiments are thus ideal for selectively observing hydrous phases in mixed-phase samples. The single-pulse ^{27}Al MAS NMR spectra of the phase egg sample have also been found to contain negligible contribution from the minor coexisting corundum, whereas those of the topaz-OH sample contain significant contributions from coexisting kyanite and are thus not reported. More details can be found in the subsequent sections. All the reported NMR spectra have been processed with an exponential line broadening function of 50 Hz to improve S/N.

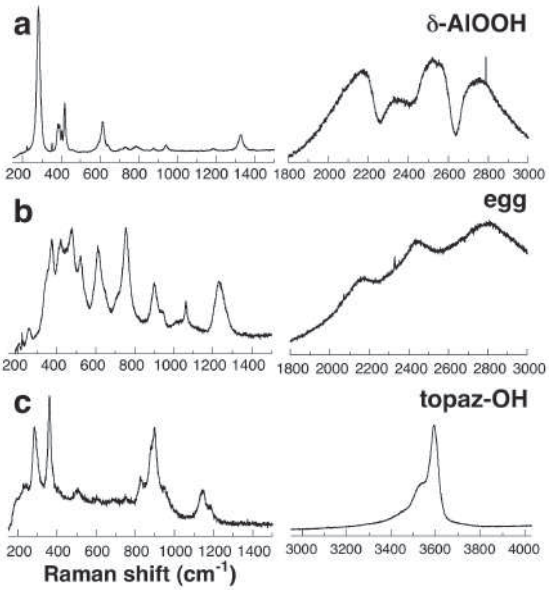

FIGURE 2. (**a**) Unpolarized Raman spectra of δ-AlOOH, (**b**) phase egg, and (**c**) topaz-OH. Vertical scale is arbitrary. Sharp spikes are due to cosmic rays.

RESULTS

Raman spectra

Representative Raman spectra for the three phases are shown in Figure 2. The pair of weak bands near 877 and 940 cm^{-1} in Figure 2a is most likely due to fluorescence, as discussed in the previous section. The weak bands near 727, 783, and 1187 cm^{-1} in Figure 2a and the sharp band near 1062 cm^{-1} in Figure 2b were not observed for all other grains, and thus could be due to contaminations or impurities; all other bands can be attributed to vibrational modes of the respective phase. The spectra of δ-AlOOH show four broad bands near 2170, 2330, 2530, and 2740 cm^{-1} for OH stretching vibrations in the 1800~3000 cm^{-1} region, and bands near 280, 385, 390, 402, 415, 613, 640, and 1330 cm^{-1} in the 200~1500 cm^{-1} region (Fig. 2a), similar to that reported previously (Ohtani et al. 2001). Kudoh et al. (2004) have interpreted the presence of multiple OH stretching bands in the latter as related to the existence of two H sites associated with Si and Mg substitution. This interpretation clearly cannot be valid, because our samples do not contain such substitutions. It is, in fact, well known that broad, multiple Raman and IR bands with low OH stretching frequencies can be observed even when a single crystallographically unique H site is present, and are characteristic of strong and very strong hydrogen bonding (Hadzi and Bratos 1976). These features are often interpreted as due to Fermi resonance between the broad fundamental OH stretching and overtones and combinations that fall within the same range, such as those of in-plane (δ_{OH}) and out-of-plane (γ_{OH}) OH bending librations, which result from anharmonicity of strong hydrogen bonds (cf. Hadzi and Bratos 1976; Hammer et al. 1998; Zarubin 1999). The band shapes in the OH stretching region resulting from Fermi resonance have been found to be quite variable and may contain up to five maxima, and the detailed interpretations are still controversial. An often-observed pattern is the so-called

ABC band containing three maxima and two minima, with the latter coinciding with $2\delta_{OH}$ and $2\gamma_{OH}$ and interpreted as transmission windows due to the disappearance of the narrow overtone bands. There are also cases when the narrow overtone band may survive, but with a shifted frequency and enhanced intensity (cf. Novak 1974; Hammer et al. 1998; Zarubin 1999). The relatively low frequencies of OH stretching vibrations [centered near 2350 cm^{-1} as compared to 2950 cm^{-1} for diaspore (Kohler et al. 1997) and 3190 cm^{-1} for boehmite (Kiss et al. 1980)], and the presence of multiple bands in this region for δ-AlOOH are both consistent with strong hydrogen bonding, as suggested from XRD refinement (O-H···O distance of 2.50~2.51 Å) (Suzuki et al. 2000; Kudoh et al. 2004). The band near 1330 cm^{-1} may be attributed to in-plane OH bending libration, based on a comparison with the corresponding bands (around 1050~1160 cm^{-1}) for diaspore (Kohler et al. 1997) and boehmite (Kiss et al. 1980). The higher frequency of the former is expected from the known inverse correlation with hydrogen bonding distance for this mode (cf. Novak 1974). Its first overtone would fall within the range observed for the OH stretching bands, and could coincide with the highest-frequency minimum (near 2630 cm^{-1}), consistent with the above interpretation of Fermi resonance. Raman bands between 280 and 640 cm^{-1} can be attributed to AlO_6 vibrations by analogy with assignments for boehmite and diaspore (e.g., Kiss et al. 1980; Kohler et al. 1997).

Raman spectra of phase egg show three broad bands near 2150, 2450, and 2800 cm^{-1} in the OH stretching region, and bands near 255, 374, 418, 474, 521, 610, 754, 898, 940, and 1232 cm^{-1} in the 200~1500 cm^{-1} region (Fig. 2b). Like δ-AlOOH, the presence of multiple broad OH stretching bands with relatively low frequencies (centered near 2440 cm^{-1}) is characteristic of strong hydrogen bonding, consistent with the reported crystal structure (O-H···O distance of 2.577 Å) (Schmidt et al. 1998). Similarly, the band near 1232 cm^{-1} may be attributed to in-plane OH bending libration. Its first overtone would fall within the range observed for OH stretching vibration, and thus may interact with the latter through Fermi resonance. Unlike δ-AlOOH, the observed minima in the OH-stretching region do not seem to correspond to the overtone frequency. Bands between 200 and 950 cm^{-1} may be attributed to vibrational modes associated with SiO_6 and AlO_6.

Raman spectra of topaz-OH exhibit two main bands near 3593 and 3525 cm^{-1} and a weak tail near 3450 cm^{-1} in the OH stretching region (see Fig. 2c), with relative intensities varying among grains, consistent with those reported previously (Komatsu et al. 2005). As revealed from previous IR and Raman studies (Wunder et al. 1993; Komatsu et al. 2005), the OH stretching frequencies of topaz-OH are somewhat lower than that of F-rich topaz (near 3650 cm^{-1}), indicating stronger hydrogen bonding of the former. Within the 200~1500 cm^{-1} region, bands near 285, 359, 504, 828, 897, 946, 1140, and 1180 cm^{-1} are observed (Fig. 2c). The bands near 1140 and 1180 cm^{-1} are likely due to in-plane OH bending libration. Shinoda and Aikawa (1997) have proposed a similar mode assignment for a single IR band near 1165 cm^{-1} in natural OH-bearing topaz [OH/(OH + F) = 10 mol%) . The detection of two OH bending bands in topaz-OH would be consistent with the presence of multiple H sites. Bands between 200 and 950 cm^{-1} may be attributed to SiO_4 and AlO_6 vibrations.

Raman spectra for stishovite and kyanite coexisting with topaz-OH (not shown) are similar to those reported previously in the 200~1500 cm^{-1} range (Mernagh and Liu 1991; Hemley et al. 1986). Within the range for OH stretching vibrations, no bands were observed for kyanite, consistent with its anhydrous nature. For stishovite, a weak band near 3120 cm^{-1} was observed, suggesting the presence of a small amount of water. This is consistent with previous IR studies that identified an absorption band at 3111 cm^{-1} (with estimated H_2O concentrations <0.1 wt%) for stishovite synthesized in the presence of Al_2O_3 and H_2O at 10~15 GPa and 1200~1400 °C (Pawley et al. 1993; Chung and Kagi 2002).

^{1}H MAS NMR results

Representative ^{1}H MAS NMR spectra for all three phases are shown in Figure 3, and a summary of all the NMR results can be found in Table 2. The ^{1}H MAS NMR spectra of the δ-AlOOH sample measured at a range of spinning rates up to 17 kHz show a single, symmetric central band near 12.5 ppm and several pairs of spinning sidebands (Fig. 3a). A small, sharp peak near 1.2 ppm is also present, and is most likely due to organic contaminations (see Yesinowski et al. 1988). Similarly, the ^{1}H MAS NMR spectra of phase egg measured at spinning rates up to 16 kHz all show a single, symmetric central band near 12.0 ppm and several pairs of spinning sidebands (Fig. 3b). The ^{1}H chemical shifts for both are larger than those of boehmite (8.8 ppm) and diaspore (10.8

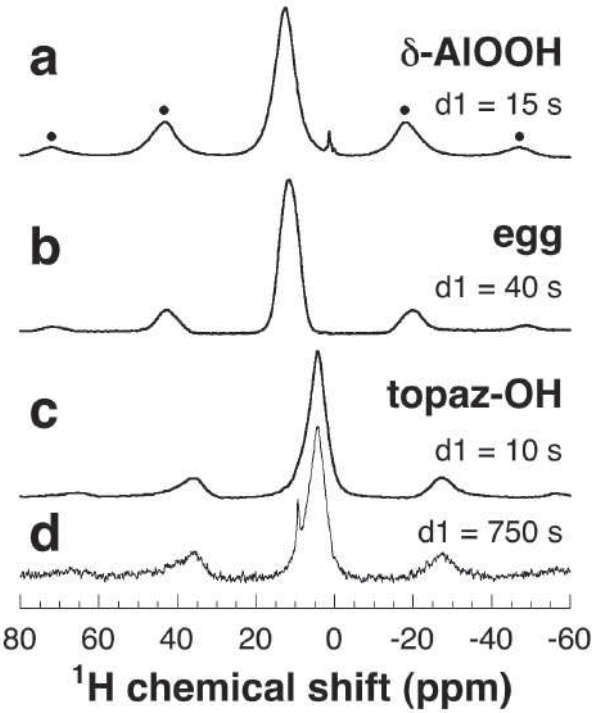

FIGURE 3. (**a**) ^{1}H MAS NMR spectra of the δ-AlOOH, (**b**) phase egg, and (**c**, **d**) topaz-OH sample, acquired with a spinning rate of 12 kHz, a spectral width of 1 or 2 MHz and recycle delay times (d1) as shown. The d1 values are all >5T_1 of the respective hydrous phase. Spinning sidebands are marked by dots. The small, sharp peak near 1.2 ppm in **a** is likely due to organic contaminations. The small, narrow peak near 9.3 ppm in **d** is due to the coexisting aluminous stishovite that has a much longer T_1.

ppm) (Piedra et al. 1996), consistent with stronger hydrogen bonding of the former, as revealed from XRD refinement and Raman spectroscopy. The full-width-at-half-maximum (FWHM) of the central band for both phases are about 5.9 ppm at 12 kHz and larger at lower spinning rates. In δ-AlOOH, each H has two nearest H neighbors at a distance of 2.833 Å, according to the H1 positions in Kudoh et al. (2004), whereas in phase egg, each H has one nearest H neighbor at a distance of 2.993 Å (Schmidt et al. 1998). The peak widths for both thus likely have large contributions from ^{1}H-^{1}H dipolar interactions that are only partially averaged by sample spinning. However, considering the fewer H nearest neighbors and longer H–H distances of the latter, it is likely that there are additional contributions to the peak width of phase egg (see further discussions below).

The ^{1}H MAS NMR spectra of the topaz-OH (+ kyanite + stishovite) sample measured at spinning rates between 10 and 15 kHz and recycle delay times of 5 to 10 s are similar and all show a single, asymmetric peak with a maximum near 4.1 ppm and a tail to higher frequency (Fig. 3c), whereas those acquired with much longer delay times (200~750 s) show an additional small, sharp peak near 9.3 ppm (Fig. 3d). Our parallel study on single-phase water-bearing aluminous stishovite confirmed that the sharp peak is due to stishovite, which has a narrow FWHM of 0.5 ppm and an extremely long T_1 of 142 s. Long ^{1}H T_1 values are typical of silicates with low H concentrations and no paramagnetic impurities (see Xue and Kanzaki 2004). The ^{1}H chemical shift (9.3 ppm) is also consistent with the observed OH stretching frequency (3120 cm^{-1}) for stishovite (see further discussions below). The broad, asymmetric peak in the ^{1}H MAS NMR spectra acquired with delay times of 5~10 s (Fig. 3c) can be attributed to topaz-OH; these short delay times have rendered stishovite invisible due to severe saturation, while still allowing full relaxation for topaz-OH. Thus, a judicious choice of recycle delay time makes it possible to selectively observe signals from topaz-OH in the mixed-phase sample. This point becomes important for the interpretation of the ^{1}H-^{29}Si and ^{1}H-^{27}Al CP-MAS NMR spectra described below. The maximum (4.1 ppm) of the observed ^{1}H NMR peak for topaz-OH is close to, though somewhat larger than that reported for a natural topaz close to the F- end-member composition (3.0 ppm) (Yesinowski et al. 1988), consistent with stronger hydrogen bonding of topaz-OH, as described above. The asymmetric peak shape suggests the presence of a range of hydrogen bonding distances, again in accord with the Raman and IR results described above.

^{1}H-^{29}Si CP-MAS NMR results

Typical ^{1}H-^{29}Si CP-MAS NMR spectra for phase egg and topaz-OH samples are shown in Figure 4. The spectra for phase egg, acquired with contact times between 0.2 and 20 ms and recycle delay times of 1 to 3 s, all show two partially overlapping peaks with maxima near –183.4 and –173.5 ppm, and an additional, smaller shoulder to higher frequency (Fig. 4a). These peaks roughly fall within the range known for octahedral Si in silicates (–166.6 to –221 ppm) (cf. Stebbins and Kanzaki 1991; Phillips et al. 1997), but do not agree with data for any known silicate phases in the Al_2O_3-SiO_2-H_2O system (e.g., –191.4 ppm for SiO_2 stishovite: Xue et al. 1993). Together with the XRD result, we can confidently attribute all three peaks to structural

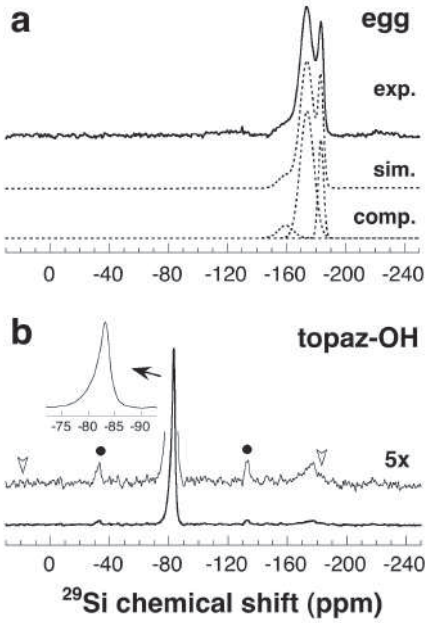

FIGURE 4. (**a**) ^{1}H-^{29}Si CP-MAS NMR spectra of phase egg and (**b**) topaz-OH, both acquired with a spinning rate of 4 kHz, a contact time of 8 ms and a recycle delay time of 3 s. Also shown in **a** are the simulated spectrum and individual Gaussian components. The spectrum above **b** is an expanded view with the vertical scale enlarged by 5×. The inset is the expanded region around the –83.3 ppm peak for **b**. Dots denote observed spinning sidebands, and open arrows indicate positions expected for spinning sidebands. The broad peak near –177 ppm in **b** is clearly not a spinning sideband.

Si in phase egg. The absence of a peak from the minor stishovite may be explained by its small abundance coupled with low CP efficiency (see below). Relative intensities of CP-MAS NMR spectra normally do not reflect the site abundance ratios, unless all peaks have similar CP dynamics. The intensities of all three peaks of phase egg increase with contact time up to about 8 ms and then level off between 8 and 20 ms. We have simulated all the spectra acquired with contact times of 2~20 ms and recycle delays of 1~3 s. Because simulations with unconstrained Lorentzian/Gaussian lineshape yielded Gaussian fractions >0.9 for all three peaks, and also gave abundance results similar to those using pure Gaussian functions (within uncertainties of the latter results), we have chosen to report the simulation results using pure Gaussian components. The simulation results for all the spectra are similar, and thus only the average values are reported (see Table 2). A comparison of the experimental and simulated spectra, and the individual Gaussian components is shown in Figure 4a. The insensitivity of the relative peak intensities to contact time over a range of values between 2 to 20 ms suggests that they reflect the true abundance ratios. The estimated T_{SiH} for the main peaks near –173.8 and –183.4 ppm are 1.60 and 1.57 ms, respectively. These values are much shorter than those of octahedral Si in high-pressure hydrous magnesium silicates, phase B and superhydrous B (= phase C) (16 and 27 ms) (Phillips et al. 1997), consistent with the shorter Si-H distances of

the former. However, in the reported crystal structure of phase egg (Schmidt et al. 1998), there is only a single Si and single Al site in the unit cell: each Si has 3Si and 6Al NNN and each Al has 6Si and 3Al NNN. The identification of multiple ^{29}Si NMR peaks suggests that the crystal structure refined from powder XRD needs to be reconsidered. The most plausible explanation is that the distribution of Si and Al over the two octahedral sites may be partially disordered, which would result in Si sites with different NNN Si/Al ratios, as was often observed for tetrahedral Si-Al distributions in low-pressure minerals (cf. Kirkpatrick 1988). Detailed assignment of NNN to the observed peaks will be discussed in the next section.

The ^{1}H-^{29}Si CP-MAS NMR spectra of the topaz-OH sample acquired with contact times between 0.2 and 20 ms and a delay time of 3 s all show an asymmetric peak with a maximum near –83.3 ppm and a tail to higher frequency, attributable to topaz-OH (see Fig. 4b). The position of this peak is somewhat less negative than that reported for a natural F-rich topaz (–85.6 ppm: Mägi et al. 1984), but instead close to those of kyanite (–83.2 and –82.3 ppm: Sherrif and Grundy 1988) that has a similar local structure around SiO_4. The estimated T_{SiH} for this peak is 1.3 ms, similar to those of phase egg, and $T_{1\rho}$(H) is 83 ms. In addition, there is a small, broad peak near –177 ppm with an integrated intensity of about 7%. As is clear from Figure 4b, this peak cannot be attributed to the spinning sideband of the –83.3 ppm peak, and thus must be due to the presence of a small amount of octahedral Si. Although this peak falls within the range observed for phase egg, it is unlikely to be due to the latter, because we did not observe any diffraction lines of phase egg from careful XRD analysis and the NMR peak shapes are also somewhat different. Contribution from the coexisting stishovite is also unlikely, because it would yield a sharp peak near –191.3 ppm. The short recycle delay time (3 s) used in these experiments would have saturated signals from stishovite (see above). In addition, the CP efficiency of stishovite is expected to be much lower than topaz-OH, considering its much lower water content. Previous IR studies on stishovite synthesized in the presence of Al_2O_3 and H_2O under similar *P-T* conditions (10~15 GPa and 1200~1400 °C) (Pawley et al. 1993; Chung and Kagi 2002) have reported that the water contents are <0.1 wt%, which are more than two orders of magnitude lower than that of topaz (about 10%). Thus, the most plausible source for the observed octahedral Si is topaz-OH, which would imply a small degree of Si-Al disorder because no Si excess was revealed from electron microprobe analysis (Si/Al = 0.43: see Table 1). Partial occupancy of octahedral sites by Si is typical of high-pressure phases, and has been recognized in $MgSiO_3$ majorite (Angel et al. 1989; Phillips et al. 1992) and sodium-bearing pyroxenes of $Na(Mg_{0.5}Si_{0.5})^{VI}Si^{IV}{}_2O_6$ (Angel et al. 1988; Stebbins and Kanzaki 1991) and $(Ca_{0.36}Na_{0.56}Mg_{0.08})(Mg_{0.73}Si_{0.27})^{VI}Si^{IV}{}_2O_6$ (Yang and Konzett 2005).

^{27}Al MAS and ^{1}H-^{27}Al CP-MAS NMR results

Single-pulse ^{27}Al MAS NMR spectra of δ-AlOOH and phase egg, and ^{1}H-^{27}Al CP-MAS NMR spectra of phase egg and topaz-OH are shown in Figure 5. As described above, the single-pulse ^{27}Al MAS NMR spectra contain a small, sharp peak near 103.8 ppm due to AlN impurity in the silicon nitride rotor. Nevertheless, the ST spinning sidebands of both phases are reasonably resolved from those due to the rotor (see inset in Fig. 5a for an expanded view of δ-AlOOH), and thus their intensity patterns are not significantly affected. For δ-AlOOH, both the ST spinning sideband intensity pattern and the central band shape (after background subtraction) can be reasonably simulated by a single Al site with a C_Q of 3.35 (0.05) MHz, η_Q of 0.88 (0.03) and δ_i^{Al} of 13.4 (0.5) ppm (see Figs. 5a and 5b). The estimated δ_i^{Al} value is similar to those reported for low-pressure aluminum hydroxides (9.1~17.2 ppm: Damodaran et al. 2002).

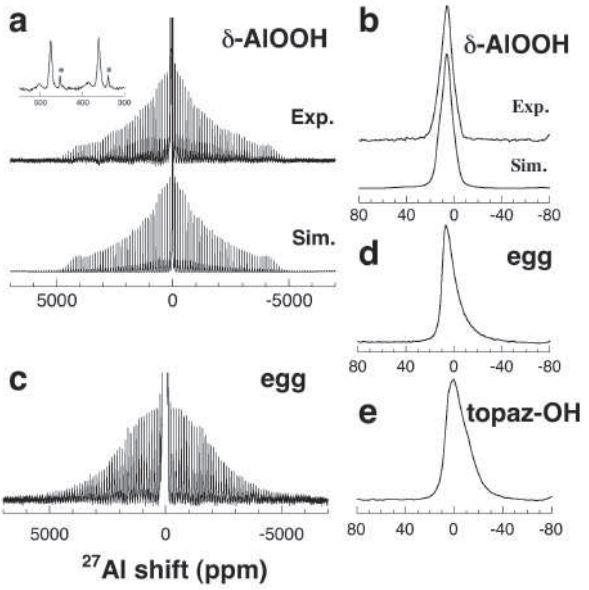

FIGURE 5. (**a**) Single-pulse ^{27}Al MAS NMR spectra of δ-AlOOH showing the entire spinning sideband pattern and (**b**) the region around the central band, after background subtraction, (**c**) single-pulse ^{27}Al MAS NMR spectrum, and (**d**) ^{1}H-^{27}Al CP-MAS NMR spectrum of phase egg, as well as (**e**) ^{1}H-^{27}Al CP-MAS NMR spectrum for topaz-OH. The simulated spectra for δ-AlOOH are shown below the experimental data. Inset above **a** is the expanded view of the region of the left third- and forth- order spinning sidebands, with peaks due to AlN impurity in the silicon nitride rotor marked by asterisks. These spectra were all acquired with the Jakobsen 5 mm probe, at a spinning rate of 12 kHz and recycle delay of 1 s for the single-pulse spectra, and a spinning rate of 10 kHz, contact time of 2 ms and recycle delay of 3 s for the CP spectra.

For phase egg, contribution from the coexisting corundum to the single-pulse ^{27}Al NMR spectra must be negligible, considering its very low abundance and the similarity in central band shape, after background subtraction (not shown), with the ^{1}H-^{27}Al CP-MAS NMR spectrum (see Fig. 5d). Both spectra show an asymmetric peak with a maximum near 6.4 ppm and a tail to lower frequency. The ST spinning sideband intensities of phase egg in the single-pulse ^{27}Al NMR spectra show a bell-shaped pattern with no well-defined fine structures (see Fig. 5c). From the average of the positions of the ST spinning sideband pairs [11.9 (0.5) ppm], and the center of gravity of the central band [5.4 (0.2) ppm from both CP-MAS and background-subtracted single-pulse spectra], the mean δ_i^{Al} and C_Q can be estimated to be about 11.2 ppm and 3.0 MHz, respectively (cf. Jäger et al. 1992), similar to those of δ-AlOOH. Unlike the latter, however, neither the central band nor the ST spinning sideband intensi-

ties for phase egg can be simulated with a single quadrupolar pattern, although the reported crystal structure by Schmidt et al. (1998) contains only a single Al site. Both in fact resemble those typically observed for glasses and disordered crystalline phases (e.g., mullites), which have been reproduced using a distribution of quadrupolar interaction parameters (cf. Jäger 1994). Thus, the ^{27}Al NMR spectra of phase egg are consistent with the presence of structural disorder, as inferred from the ^{29}Si NMR data.

For the topaz-OH sample, the ^{1}H-^{27}Al CP-MAS NMR spectra acquired with contact times of 0.1~8 ms are similar and all show an asymmetric peak with a maximum near –0.8 ppm, attributable to topaz-OH (Fig. 5e) (the single-pulse ^{27}Al MAS NMR spectra contained additional peaks due to kyanite and is not shown). Like phase egg, the central band of topaz-OH cannot be satisfactorily simulated with a single set of parameters, indicating the presence of local structural disorder. An approximate simulation gives a rough estimation of a mean δ_i^{Al} of 10 ppm, C_Q of 4.5 MHz, and η_Q of 0.7. The estimated δ_i^{Al} value is similar to those of octahedral Al in the other hydrous phases described above. It is somewhat puzzling that there are no obvious peaks in the 50~90 ppm range expected for tetrahedral Al (cf. Stebbins 1995) in the ^{1}H-^{27}Al CP-MAS NMR spectra, although its presence (a few percent) is implied from the ^{29}Si NMR data described above. The ^{27}Al C_Q is known to be very sensitive to the distortion of the coordination polyhedron, exhibiting a large range of values (cf. Skibsted et al. 1993; Stebbins 1995). Thus, if the tetrahedral Al has a much larger C_Q than those of the octahedral Al as a result of local structure distortion, it would be difficult to detect at a low abundance of a few percent. Further experimental and theoretical studies are necessary to clarify this matter.

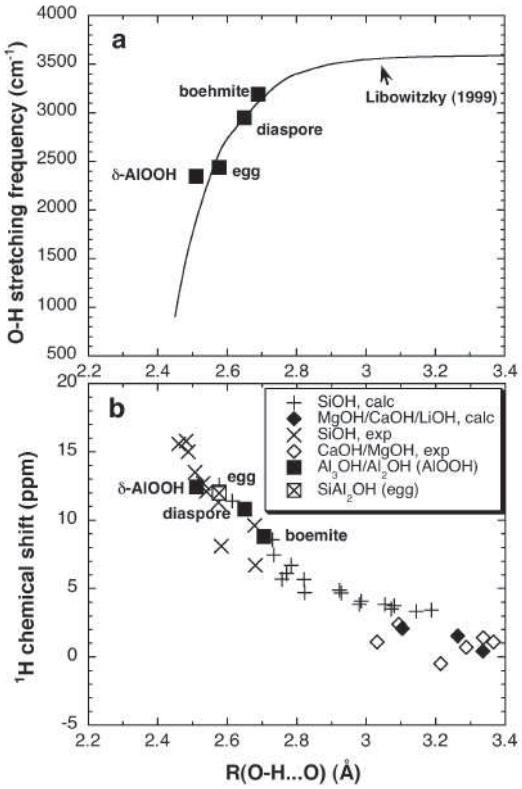

FIGURE 6. (**a**) OH stretching frequency and (**b**) ^{1}H chemical shift as a function of O-H···O distance. Plotted in both are experimental data for δ-AlOOH, phase egg (this study), and boehmite and diaspore (OH frequency: Kiss et al. 1980; Kohler et al. 1997; NMR: Piedra et al. 1996). Also shown in **a** is the correlation derived from experimental data (Libowitzky 1999), and in **b** are experimental data for SiOH, CaOH, and MgOH groups in crystalline silicate phases compiled in Xue et al. (2004) and reported by Johnson and Rossman (2004), as well as ab initio calculation results for small clusters from Xue et al. (2004).

DISCUSSION

Hydrogen bonding in δ-AlOOH, phase egg, and topaz-OH

It is well known from experimental studies and theoretical calculations that the OH stretching frequency and ^{1}H chemical shift both exhibit good correlations with the O-H···O and H···O distances, although dependency on other parameters, such as the cation type and bifurcation of H bonds, becomes more prominent for weak hydrogen bonding (cf. Nakamoto et al. 1955; Novak 1974; Libowitzky 1999; Eckert et al. 1988; Xue and Kanzaki 2004 and references therein) (also see Fig. 6). Vibrational spectroscopy has the advantage of being able to probe the spatial distributions and orientations of OH vectors, but suffers from (1) complications with spectral interpretation and difficulty in accurately determining the OH stretching frequency for strongly hydrogen-bonded OH groups due to anharmonicity and Fermi resonance and (2) complications with quantification because of the frequency- and compositional-dependency of peak intensity. A combination of the two is an ideal strategy.

In Figures 6a and 6b, we have plotted both sets of data for δ-AlOOH, phase egg (this study), and boehmite and diaspore (OH frequency: Kiss et al. 1980; Kohler et al. 1997; NMR: Piedra et al. 1996), which show good agreement with the known trends exhibited by other minerals and ab initio calculation results (OH frequency: Libowitzky 1999; NMR: Xue and Kanzaki 2004; Johnson and Rossman 2004). An O-H···O distance of 2.511 Å for δ-AlOOH (Kudoh et al. 2004), and 2.577 Å for phase egg (Schmidt et al. 1998) have been adopted in these plots. The OH stretching frequencies of 3450~3593 cm^{-1} and the asymmetric ^{1}H MAS NMR peak with a maximum near 4.1 ppm for topaz-OH both correspond to a range of O-H···O distances around 3 Å (see Fig. 6), in broad agreement with the crystal structural determination (Northrup et al. 1994). Also from these correlations, we expect an O-H···O distance around 2.68 Å for the small amount of water in aluminous stishovite. This H-bond distance is consistent with IR frequencies and Raman shifts (3111~3120 cm^{-1}) as well as ^{1}H chemical shifts (9.3 ppm). A recent first principles calculation suggested that δ-AlOOH might have symmetric (H-centered) hydrogen bonding under ambient condition (Panero and Stixrude 2004). However, the observed ^{1}H chemical shift (12.5 ppm) is much too small, and the OH stretching frequency (~2350 cm^{-1}) too high to be considered symmetric. For symmetric hydrogen bonds O-H···O distances are in the range 2.41~2.46 Å (>15 ppm and <1000 cm^{-1} respectively) (cf. Novak 1974; Emsley 1980; also see Fig. 6). The same conclusion may be drawn for phase egg. It is possible, though, that with increasing pressure, the O-H···O distances in both phases will decrease and may

eventually transform into a symmetric configuration (Tsuchiya et al. 2002; Vanpeteghem et al. 2003). Such a behavior is well known for H_2O ice, which transforms from asymmetrically hydrogen-bonded ice VII to symmetrically bonded ice X at around 70 GPa (e.g., Goncharov et al. 1996; Wolanin et al. 1997). The compression behavior and bulk modulus may be significantly affected by changes in hydrogen bonding (e.g., Goncharov et al. 1996; Tsuchiya et al. 2002).

The strong hydrogen bonding in δ-AlOOH and phase egg may be an important factor in stabilizing these structures at high pressure and temperature. Disorder in H positions and the corresponding distribution in hydrogen bonding distances for topaz-OH and, possibly also for phase egg (see below), may also contribute to their stability through increased configurational entropy. This issue will be further explored in the subsequent sections.

Si-Al ordering in phase egg

The detection of three peaks (–183.4, –173.8, –158.2 ppm) in the ^{1}H-^{29}Si CP-MAS NMR spectra of phase egg suggests the presence of significant Si-Al disorder. For tetrahedral Si, it is well known that the replacement of NNN Si by Al (or other low field strength cations such as Mg) results in systematically less negative ^{29}Si NMR chemical shifts (cf. Kirkpatrick 1988). A similar trend must also apply to octahedral Si, because all three peaks of phase egg, which most likely correspond to Si with mixed Si and Al NNN (see discussions below), have less negative chemical shifts than the structurally similar SiO_2 stishovite (–191.3 ppm). Furthermore, octahedral Si in phase B and superhydrous B, which have only octahedral Mg NNN, had been known to produce the least negative chemical shifts (–166.6 and –170.0 ppm) among octahedral Si (Phillips et al. 1997). Thus, we may attribute the –158.2, –173.8, and –183.4 ppm peak of phase egg to Si with increasing NNN Si/Al ratio. The degree of disorder (fraction of Si in the Al site, or vice versa) must be significantly less than 0.5, otherwise the assignment of Si and Al in the structural refinement from XRD, based on bond valence considerations (see Schmidt et al. 1998), would have been difficult. We will use these observations as well as the fact that the peak width increases toward less negative chemical shift as constraints in the subsequent modeling. The simplest model is to assume that (1) Si and Al are distributed randomly over the two octahedral sites, and (2) Si with the same number of Si and Al NNN gives similar ^{29}Si chemical shifts, regardless of which of the two sites it occupies. In the structure of phase egg, each SiO_6 (or AlO_6) is linked to three other octahedra by edge sharing and six others by corner sharing. Detailed assignment depends on whether Si-Al disorder at corner-sharing or edge-sharing NNN sites impose greater (or comparable) influence on the ^{29}Si chemical shift. As further discussed below, there is indirect evidence suggesting that the latter has dominant effects. As an independent evaluation, we have quantitatively modeled all three extreme cases: (1) edge- and corner-sharing NNN sites have comparable influence, (2) corner-sharing, and (3) edge-sharing NNN sites have dominant influence. For case 1, the random mixing model predicts four species of significant abundance (within the range of small degrees of disorder): the dominant one due to Si(3Si6Al), and three others due to Si(2Si7Al), Si(4Si5Al), and Si(5Si4Al) (where numbers

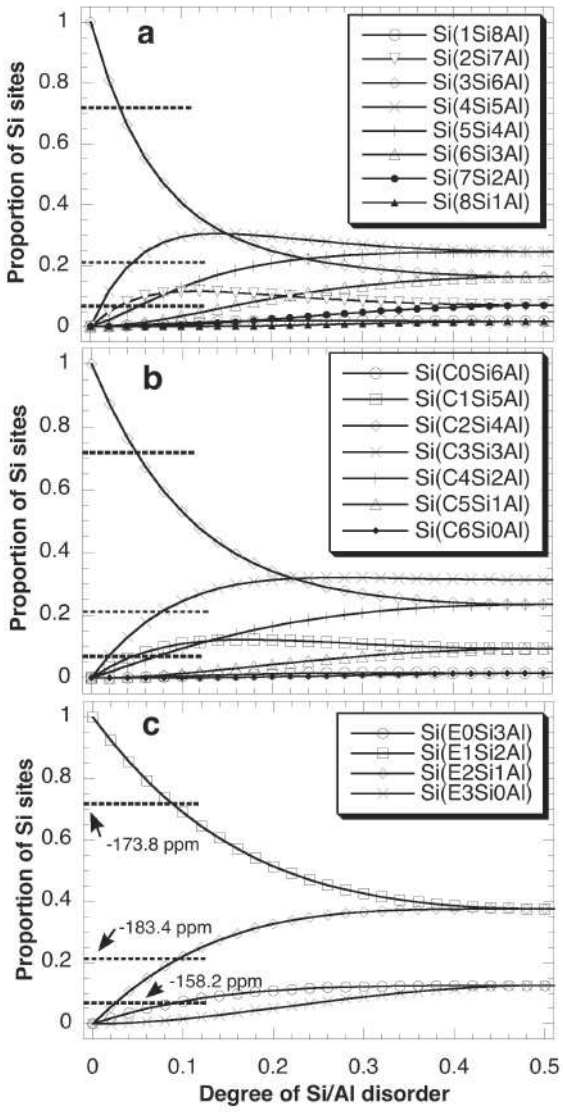

FIGURE 7. (**a**) Estimated fractions of Si sites with *n*Si and (9 – *n*)Al NNN (both corner and edge- sharing) (*n* = 1~8) (*n* = 0 and 9 both have fractions ≤0.002 and are omitted for clarity), (**b**) Si sites with nSi and (6 – *n*)Al corner-sharing NNN (*n* = 0~6), and (**c**) Si sites with nSi and (3 – *n*)Al edge-sharing NNN (*n* = 0~3), as a function of the degree of Si-Al disorder, assuming random mixing. The horizontal broken lines indicate the observed relative abundances of the three ^{29}Si NMR peaks of phase egg, and their thickness represents the extent of uncertainties.

stand for total number of edge- and corner-sharing NNN), with relative proportions shown in Figure 7a. The Si(2Si7Al) and Si(5Si4Al) species may be considered to contribute to the –158.2 and –183.4 ppm peak, respectively, and the dominant Si(3Si6Al) species to the most intense –173.8 ppm peak. There are two possibilities for the Si(4Si5Al) species, contributing either to the –183.4 or the –173.8 ppm peak. However, the former cannot account for the narrowest width of the –183.4 ppm peak, and the latter cannot explain the observed relative intensities for the three NMR peaks. Similarly, case 2 predicts significant

abundances for three Si species, Si(C1Si5Al), Si(C3Si3Al), and Si(C4Si2Al), in addition to the dominant Si(C2Si4Al) species (where C stands for corner-sharing NNN) (see Fig. 7b), which cannot simultaneously account for the relative intensities and widths of the three observed peaks. On the other hand, case 3 predicts three Si species of significant abundance, Si(E1Si2Al), Si(E2Si1Al), and Si(E0Si3Al) (where E stands for edge-sharing NNN), which may contribute to the –173.8, –183.4, and –158.2 ppm peak, respectively. Their relative abundances at a degree of disorder of 0.1 agree well with the experimental data (see Fig. 7c). The observed increasing peak width toward less negative chemical shift may be explained by greater secondary contribution from disorder at the corner-sharing NNN cation sites, with decreasing Si/Al ratio at the edge-sharing NNN sites. Thus, our quantitative modeling suggests that (1) disorder at the edge-sharing cation sites has a predominant influence on the ^{29}Si chemical shift, and (2) the degree of Si-Al disorder in phase egg is about 10%.

Si-Al disorder is expected to affect the H positions in phase egg. In the fully ordered structure, there are four O sites: O1 and O2 are each bonded to 2Si1Al, and O3 and O4 to 1Si2Al. A H bond is formed O3 and O4, which have the lowest bond valence sums (O4-H···O3). With 10% random Si-Al disorder, the populations of O3 and O4 sites bonded to 1Si2Al are each reduced to 75%, and those bonded to 1Al2Si (16%), 3Al0Si(8%), and 0Al3Si (1%) are developed. Likewise, O1 and O2 sites bonded to 1Al2Si are reduced (75%), and those bonded to 2Al1Si (16%), 0Al3Si (8%), and 3Al0Si (1%) are developed. It is likely from bond valence considerations that H atoms tend to be close to O atoms with low bond valence sums (OAl_2Si, OAl_3), so that some of the H atoms may be located in positions different from those in the ordered structure. Disorder in H positions could be partially responsible for the observed large width of the ^{1}H MAS NMR peak for phase egg. The lack of multiple peaks could be a result of relatively small dispersions in chemical shift, as is observed between δ-AlOOH and phase egg.

Cation disorder and H positional disorder would increase the configurational entropy and affect the physical and thermodynamic properties and stability field of phase egg. The unusually high upper temperature stability limit (up to about 1700 °C) of phase egg (see Ono 1999; Sano et al. 2004) is noteworthy in this regard. This is most likely the combined outcome of structural disorder and strong hydrogen bonding, both of which enhance high-temperature stability of phase egg. This feature renders phase egg an important water reservoir not only in cold subducted slabs, but also along normal mantle geotherm (cf. Sano et al. 2004). Furthermore, because phase egg possesses a composition at the midpoint between δ-AlOOH and stishovite, the observation of Si-Al disorder in phase egg implies that mutual solubility between the latter two components is energetically favorable. This is in accord with the experimental observations of Al and H incorporation in stishovite (see above) and Si (and Mg) in δ-AlOOH (Suzuki et al. 2000). The incorporation of water in aluminous stishovite is of particular interest, because it could be a promising water reservoir beyond the stability fields of phase egg (for normal geotherm) and δ-AlOOH (for cold subducted slabs). Previous experimental studies have reported that the Al_2O_3 content in stishovite increases significantly with temperature to about 7~9 wt% at 1600~1700 °C and 20~21 GPa, although the water contents were not determined (Ono 1999, Sano et al. 2004). A first principles calculation on the stishovite-δ-AlOOH solid solution suggested that the solubility of AlOOH component in stishovite increases with both temperature and pressure (Panero and Stixrude 2004). As the solubilities of Al and H in stishovite increase, we may anticipate development of local structures with clustered Al distributions (OAl_2Si) and perhaps also H sites with strong H bonding, similar to those in phase egg. Such an increase in the variety of structural units and strength of hydrogen bonding would further stabilize water-bearing aluminous stishovite to elevated temperatures.

Structural disorder in topaz-OH

The ^{1}H MAS, ^{1}H-^{29}Si, and ^{1}H-^{27}Al CP-MAS NMR spectra of topaz-OH are all indicative of a range of local structural parameters (bond distances and angles) around H, tetrahedral Si, and octahedral Al, rather than a single well-defined site for each, as expected from an ordered *Pbnm* structure. A long-range ordered distribution of H over two nonequivalent sites with a symmetry of $Pbn2_1$, as proposed by Northrup et al. (1994), also cannot account for the observed NMR spectra, because one would then expect only a single well-defined tetrahedral Si site. A random distribution of H over two or more sites, accompanied by a range of local structural parameters around tetrahedral Si and octahedral Al sites, as suggested from recent ab initio calculations (Churakov and Wunder 2004), would be consistent with the NMR observations.

In addition, our ^{29}Si NMR results suggest the presence of a small amount of octahedral Si, which is most likely an indication of Si-Al disorder. Like phase egg, Si-Al disorder and H positional disorder would have important implications as to the physical and thermodynamic properties of topaz-OH, and could be partly responsible for its relatively high temperature (up to 1500 °C) stability field (see Ono 1999).

Variation of ^{29}Si chemical shift with structure for octahedral Si

Tetrahedral Si in silicates shares only corners with other tetrahedral or octahedral Si or Al. For them, extensive NMR studies have revealed a systematic dependency of ^{29}Si chemical shift on local structural parameters, such as Q^n speciation, NNN Si/Al ratio, and Si-O-T (Si or Al) angle (cf. Kirkpatrick 1988; Stebbins 1995). It has also been proposed that quantitative correlations exist between ^{29}Si chemical shift and composite structural parameters, such as the magnetic susceptibility parameter, that are a function of bond distances, angles and bond valences of NNN cations (see Scherriff and Grundy 1988), have also been proposed. For octahedral Si, Stebbins and Kanzaki (1991) have similarly proposed correlations between ^{29}Si chemical shift and structural parameters, including the magnetic susceptibility term, on the basis of limited data. However, it has been found for phase B and superhydrous B that observed and predicted shifts disagree by 5 to 10 ppm (Phillips et al. 1997). Similarly, the ^{29}Si chemical shift predicted from this correlation for phase egg using the structure of Schmidt et al. (1998) is –184.7 ppm, about 11 ppm from the observed value (–173.8 ppm) for the most intense peak. Thus, quantitative modeling of the ^{29}Si chemical

shift for octahedral Si is a task yet to be accomplished. Here we will rather concentrate on the qualitative correlations because our ongoing systematic NMR investigation of other important high-pressure silicate phases is expected to expand the database in the near future.

Structural variations for octahedral Si are more diverse than tetrahedral Si, because the former can share not only corners, but also edges with other Si (and Al, Mg). It has been noted previously from limited data for high-pressure silicates that SiO_6 octahedra sharing edges with one another tend to give more negative chemical shifts (down to about –181.0 ppm for $MgSiO_3$ ilmenite) than those sharing only corners (Stebbins and Kanzaki 1991; Kanzaki et al. 1992). The data reported by Phillips et al. (1997) on phase B and superhydrous B extended the known range of ^{29}Si chemical shift for octahedral Si to –166.6 ppm and confirmed the trend of decreasing shielding with increasing edge-sharing. Our result for phase egg is a unique new addition to this database because it is the first phase studied by NMR that contains interconnected SiO_6 and AlO_6 octahedra, and it also further extends the range to –158.2 ppm, which is very close to the value (–150.0 ppm) known for pentacoordinate Si in silicate glasses (Xue et al. 1989, 1991) and α-$Ca_2Si_2O_5$ (Kanzaki et al. 1991; Stebbins and Poe 1999).

Noteworthy is the much larger range in chemical shift (33 ppm) for octahedral Si sharing one or more edges with other octahedra (SiO_6, AlO_6, or MgO_6) (from –191.3 ppm for stishovite to –158.2 ppm for phase egg) than the range (about 12 ppm) for those sharing only corners (from –191.7 ppm for $MgSiO_3$ perovskite to –203.4 ppm for K_2SiO_4 wadeite; excluding data for low-pressure PO_4-containing phases) (see data in Stebbins and Kanzaki 1991; Kanzaki et al. 1992, 1998; Phillips et al. 1997). This suggests that edge-sharing neighbors impose greater influences on the ^{29}Si chemical shift than corner-sharing neighbors, which is also supported by our modeling of phase egg (above). The same trend is also known for thiosilicates in which SiS_4 tetrahedra can share 0 to 2 edges with other SiS_4 tetrahedra and share the remaining corners with either SiS_4 or network-modifying cations (e.g., Li). In this case, the ^{29}Si chemical shifts are dominated by the number of shared edges, i.e., with each increase (from 0 to 1 to 2) in the number of shared edges the ^{29}Si chemical shift increases by more than 10 ppm. Note that the type of corner-sharing cations (Si or Li, Na) has only a secondary influence on the chemical shift in these structures (e.g., Eckert et al. 1989). The predominant influences of edge-sharing cation neighbors are understandable, considering their much shorter Si-Si (Al) distances.

ACKNOWLEDGMENTS

We thank Takuya Matsuzaki for assistance with electron microprobe analyses, and two anonymous reviewers for helpful comments. This study was supported by Grants-in-Aid for Scientific Research and the COE-21 Program, both funded by the Ministry of Education, Culture, Sports, Science and Technology of Japan. Part of this work was carried out during the Misasa International Student Intern Program 2005.

REFERENCES CITED

Angel, R.J., Finger, L.W., Hazen, R.M., Kanzaki, M., Weidner, D.J., Liebermann, R.C., and Veblen, D.R. (1989) Structure and twinning of single-crystal $MgSiO_3$ garnet synthesized at 17 GPa and 1800 °C. American Mineralogist, 74, 509–512.

Chung, J.I. and Kagi, H. (2002) High concentration of water in stishovite in the MORB system. Geophysical Research Letters, 29, 2020, DOI: 10.1029/2002GL015579.

Churakov, S.V. and Wunder, B. (2004) Ab-initio calculations of the proton location in topaz-OH, $Al_2SiO_4(OH)_2$. Physics and Chemistry of Minerals, 31, 131–141.

Cory, D.G. and Ritchey, W.M. (1988) Suppression of signals from the probe in Bloch decay spectra. Journal of Magnetic Resonance, 80, 128–132.

Damodaran, K., Rajamohanan, P.R., Chakrabarty, D., Racherla, U.S., Manohar, V., Fernandez, C., Amoureux, J.P., and Ganapathy, S. (2002) Triple-quantum magic angle spinning ^{27}Al NMR of aluminum hydroxides. Journal of the American Chemical Society, 124, 3200–3201.

Eckert, H., Yesinowski, J.P., Silver, L.A., and Stolper, E.M. (1988) Water in silicate glasses: Quantitation and structural studies by ^{1}H solid echo and MAS-NMR methods. Journal of Physical Chemistry, 92, 2055–2064.

Eckert, H., Kennedy, J.H., Pradel, A., and Ribes, M. (1989) Structural transformation of thiosilicate glasses: ^{29}Si MAS-NMR evidence for edge-sharing in the system Li_2S-SiS_2. Journal of Non-Crystalline Solids, 113, 287–293.

Eggleton, R.A., Boland, J.N., and Ringwood, A.E. (1978) High-pressure synthesis of a new aluminum silicate: $Al_5Si_3O_{17}OH$. Geochemical Journal, 12, 191–194.

Emsley, J. (1980) Very strong hydrogen bonding. Chemical Society Reviews, 9, 91–124.

Goncharov, A.F., Struzhkin, V.V., Somayazulu, M.S., Hemley, R.J., and Mao, H.K. (1996) Compression of ice to 210 gigapascals: Infrared evidence for s symmetric hydrogen-bonded phase. Science, 273, 218–220.

Hadzi, D. and Bratos, S. (1976) Vibrational spectroscopy of the hydrogen bond. In P. Schuster, G. Zundel, and C. Sandorfy, Eds., The Hydrogen Bond—Recent Developments in Theory and Experiments, p. 565–611. North-Holland Publishing Company, Amsterdam.

Hammer, V.M.F., Libowitzky, E., and Rossman, G.R. (1998) Single-crystal IR spectroscopy of very strong hydrogen bonds in pectolite, $NaCa_2[Si_3O_8(OH)]$, and serandite, $NaMn_2[Si_3O_8(OH)]$. American Mineralogist, 83, 569–576.

Hemley, R.J., Mao, H.-K., and Chao, E.C.T. (1986) Raman spectrum of natural and synthetic stishovite. Physics and Chemistry of Minerals, 13, 285–290.

Irifune, T., Kuroda, K., and Unemoto, M. (1995) Experimental study of the decomposition of kyanite at high pressure and high temperature. In T. Yukutake, Ed., The Earth's Central Part: Its Structure and Dynamics, p. 35–44. Terra Scientific Publishing Company, Tokyo.

Izumi, F. (2005) VENUS system for three-dimensional visualization of crystal structures and electronic states. Rigaku Journal, 36, 18–27 (in Japanese).

Jäger, C. (1994) Satellite transition spectroscopy of quadrupolar nuclei. In P. Diehl, E. Fluck, H. Günther, R. Kosfeld, and J. Seeing, Eds., NMR Basic Principles and Progress, 31, p. 133–170. Springer-Verlag, Berlin.

Jäger, C., Müller-Warmuth, W., Mundus, C., and Wüllen, L.V. (1992) ^{27}Al MAS-NMR spectroscopy of glasses: new facilities by application of "SATRAS". Journal of Non-Crystalline Solids, 149, 209–217.

Johnson, E.A. and Rossman, G.R. (2004) An infrared and ^{1}H MAS NMR investigation of strong hydrogen bonding in ussingite, $Na_2AlSi_3O_8(OH)$. Physics and Chemistry of Minerals, 31, 115–121.

Kanzaki, M., Stebbins, J.F., and Xue, X. (1991) Characterization of quenched high pressure phases in system $CaSiO_3$ by XRD and ^{29}Si NMR. Geophysical Research Letters, 18, 463–466.

——— (1992) Characterization of crystalline and amorphous silicates quenched from high pressure by ^{29}Si MAS NMR spectroscopy. In Y. Syono, and M.H. Manghnani, Eds. High-Pressure Research: Application to Earth and Planetary Sciences, 67, p. 89–100. Terra Scientific Publishing Company, Tokyo.

Kanzaki, M., Xue, X., and Stebbins, J.F. (1998) Phase relations in Na_2O-SiO_2 and $K_2Si_4O_9$ systems up to 14 GPa and ^{29}Si NMR study of the new high-pressure phases: Implications to the structure of high-pressure silicate glasses. Physics of the Earth and Planetary Interiors, 107, 9–21.

Kirkpatrick, R.J. (1988) MAS NMR spectroscopy of minerals and glasses. In F.C. Hawthorne, Ed., Spectroscopic Methods in Mineralogy and Geology, 18, p. 341–403. Reviews in Mineralogy, Mineralogical Society of America, Chantilly, Virginia.

Kiss, A.B., Keresztury, G., and Farkas, L. (1980) Raman and i.r. spectra and structure of boehmite (γ-AlOOH). Evidence for the recently discarded D^{17}_{2h} space group. Spectrochimica Acta, 36A, 653–658.

Kohler, T., Armbruster, T., and Libowitzky, E. (1997) Hydrogen bonding and Jahn-Teller distortion in groutite, α-MnOOH, and manganite, γ-MnOOH, and their relations to the manganese dioxides ramsdellite and pyrolusite. Journal of Solid State Chemistry, 133, 486–500.

Komatsu, K., Kagi, H., Okada, T., Kuribayashi, T., Parise, J.B., and Kudoh, Y. (2005) Pressure dependence of the OH-stretching mode in F-rich natural topaz and topaz-OH. American Mineralogist, 90, 266–270.

Kudoh, Y., Kuribayashi, T., Suzuki, A., Ohtani, E., and Kamada, T. (2004) Space group and hydrogen sites of δ-AlOOH and implications for a hypothetical high-pressure form of $Mg(OH)_2$. Physics and Chemistry of Minerals, 31, 360–364.

Libowitzky, E. (1999) Correlation of O-H stretching frequencies and O-H···O hydrogen bond lengths in minerals. Monatshefte für Chemie, 130, 1047–1059.

Mägi, M., Lippmaa, E., Samosen, A., Engelhardt, G., and Grimmer, A.R. (1984) Solid-state high-resolution silicon–29 chemical shifts in silicates. Journal of Physical Chemistry, 88, 1518–1522.

Mernagh, T.P. and Liu, L.-G. (1991) Raman spectra from the Al_2SiO_5 polymorphs at high pressures and room temperature. Physics and Chemistry of Minerals, 18, 126–130.

Nakamoto, K., Margoshes, M., and Rundle, R.E. (1955) Stretching frequencies as a function of distances in hydrogen bonds. Journal of the American Chemical Society, 77, 6480–6486.

Navrotsky, A. (1977) Calculation of effect of cation disorder on silicate spinel phase boundaries. Earth and Planetary Science Letters, 33, 437–442.

Northrup, P.A., Leinenweber, K., and Parise, J.B. (1994) The location of H in the high-pressure synthetic $Al_2SiO_4(OH)_2$ topaz analogue. American Mineralogist, 79, 401–404.

Novak, A. (1974) Hydrogen bonding in solids. Correlation of spectroscopic and crystallographic data. In J.D. Dunitz, P. Hemerich, R.H. Holm, J.A. Ibers, C.K. Jorgensen, J.B. Neilands, D. Reimene, and R.J.P. Williams, Eds., Structure and Bonding 18: Large Molecules, p. 177–216. Springer, New York.

Ohtani, E., Litasov, K., Suzuki, A., and Kondo, T. (2001) Stability field of new hydrous phase, δ-AlOOH, with implications for water transport into the deep mantle. Geophysical Research Letters, 28, 3991–3993.

Ono, S. (1999) High temperature stability limit of phase egg, $AlSiO_3(OH)$. Contributions to Mineralogy and Petrology, 137, 83–89.

Panero, W.R. and Stixrude, L.P. (2004) Hydrogen incorporation in stishovite at high pressure and symmetric hydrogen bonding in δ-AlOOH. Earth and Planetary Science Letters, 221, 421–431.

Parise, J.B., Cuff, C., and Moore, F.H. (1980) A neutron diffraction study of topaz: evidence for lower symmetry. Mineralogical Magazine, 43, 943–944.

Pawley, A.R., McMillan, P.F., and Holloway, J.R. (1993) Hydrogen in stishovite, with implications for mantle water content. Science, 261, 1024–1026.

Phillips, B.L., Howell, D.A., Kirkpatrick, R.J., and Gasparik, T. (1992) Investigation of cation order in $MgSiO_3$-rich garnet using ^{29}Si and ^{27}Al MAS NMR spectroscopy. American Mineralogist, 77, 704–712.

Phillips, B.L., Burnley, P.C., Worminghaus, K., and Navrotsky, A. (1997) ^{29}Si and ^{1}H NMR spectroscopy of high-pressure hydrous magnesium silicates. Physics and Chemistry of Minerals, 24, 179–190.

Piedra, G., Fitzgerald, J.J., Dando, N., Dec, S.F., and Maciel, G.E. (1996) Solid-state ^{1}H NMR studies of aluminum oxide hydroxides and hydroxides. Inorganic Chemistry, 35, 3474–3478.

Prewitt, C.T. and Parise, J.B. (2000) Hydrous phases and hydrogen bonding at high pressure. In R.M. Hazen and R.T. Downs, Eds., High-Temperature and High-Pressure Crystal Chemistry, 41, p. 309–333. Reviews in Mineralogy and Geochemistry, Mineralogical Society of America, Chantilly, Virginia.

Sano, A., Ohtani, E., Kubo, T., and Funakoshi, K. (2004) In situ X-ray observation of decomposition of hydrous aluminum silicate $AlSiO_3OH$ and aluminum oxide hydroxide d-AlOOH at high pressure and temperature. Journal of Physics and Chemistry of Solids, 65, 1547–1554.

Schmidt, M.W. (1995) Lawsonite: upper pressure stability and formation of higher density hydrous phases. American Mineralogist, 80, 1286–1292.

Schmidt, M.W., Finger, L.W., Angel, R.J., and Dinnebier, R.E. (1998) Synthesis, crystal structure, and phase relations of $AlSiO_3OH$, a high-pressure hydrous phase. American Mineralogist, 83, 881–888.

Sherriff, B.L. and Grundy, H.D. (1988) Calculations of ^{29}Si MAS NMR chemical shift from silicate mineral structure. Nature, 332, 819–822.

Shinoda, K. and Aikawa, N. (1997) IR active orientation of OH bending mode in topaz. Physics and Chemistry of Minerals, 24, 551–554.

Skibsted, J., Henderson, E., and Jakobsen, H.J. (1993) Characterization of calcium aluminate phases in cements by ^{27}Al MAS NMR spectroscopy. Inorganic chemistry, 32, 1013–1027.

Stebbins, J.F. (1995) Nuclear magnetic resonance spectroscopy of silicates and oxides in geochemistry and geophysics. In T.J. Ahrens, Ed., Mineral Physics and Crystallography, A Handbook of Physical Constants, p. 303–331. American Geophysical Union, Washington, D.C.

Stebbins, J.F. and Kanzaki, M. (1991) Local structure and chemical shifts for six-coordinated silicon in high-pressure mantle phases. Science, 251, 294–298.

Stebbins, J.F. and Poe, B.T. (1999) Pentacoordinate silicon in high-pressure crystalline and glassy phases of calcium disilicate ($CaSi_2O_5$). Geophysical Research Letters, 26, 2521–2523.

Suzuki, A., Ohtani, E., and Kamada, T. (2000) A new hydrous phase δ-AlOOH synthesized at 21 GPa and 1000 °C. Physics and Chemistry of Minerals, 27, 689–693.

Tsuchiya, J., Tsuchiya, T., Tsuneyuki, S., and Yamanaka, T. (2002) First principles calculation of a high-pressure hydrous phase, δ-AlOOH. Geophysical Research Letters, 29, 1909, DOI: 10.1029/2002GL015417.

Vanpeteghem, C.B., Ohtani, E., Kondo, T., Takemura, K., and Kikegawa, T. (2003) Compressibility of phase Egg $AlSiO_3OH$: Equation of state and role of water at high pressure. American Mineralogist, 88, 1408–1411.

Vega, A.J. (1992) CP/MAS of quadrupolar S = 3/2 nuclei. Solid State Nuclear Magnetic Resonance, 1, 17–32.

Wolanin, E., Pruzan, P., Chervin, J.C., Canny, B., Gauthier, M., Hausermann, D., and Hanfland, M. (1997) Equation of state of ice VII up to 106 GPa. Physical Review B, 56, 5781–5785.

Wunder, B., Rubie, D.C., Ross, C.R, II, Medenbach, O., Seifert, F., and Schreyer, W. (1993) Synthesis, stability and properties and of $Al_2SiO_4(OH)_2$: A fully hydrated analogue of topaz. American Mineralogist, 78, 285–297.

Xue, X. and Kanzaki, M. (2004) Dissolution mechanisms of water in depolymerized silicate melts: Constraints from ^{1}H and ^{29}Si NMR spectroscopy and ab initio calculations. Geochimica et Cosmochimica Acta, 68, 5027–5057.

Xue, X., Stebbins, J.F., Kanzaki, M., and Trønnes, R.G. (1989) Silicon coordination and speciation changes in a silicate liquid at high pressures. Science, 245, 962–964.

Xue, X., Stebbins, J.F., Kanzaki, M.,McMillan, P.F., and Poe, B. (1991) Pressure-induced silicon coordination and tetrahedral structural changes in alkali oxide-silica melts up to 12 GPa: NMR, Raman, and infrared spectroscopy. American Mineralogist, 76, 8–26.

Xue, X., Stebbins, J.F., and Kanzaki, M. (1993) A ^{29}Si MAS NMR study of sub-Tg amorphization of stishovite at ambient pressure. Physics and Chemistry of Minerals, 19, 480–485.

Yang, H. and Konzett, J. (2005) Crystal chemistry of a high-pressure *C*2/*c* clinopyroxene with six-coordinated silicon. American Mineralogist, 90, 1223–1226.

Yesinowski, J.P., Eckert, H., and Rossman, G.R. (1988) Characterization of hydrous species in minerals by high-speed ^{1}H MAS-NMR. Journal of the American Chemical Society, 110, 1367–1375.

Zarubin, D.P. (1999) Infrared spectra of hydrogen bonded hydroxyl groups in silicate glasses. A re-interpretation. Physics and Chemistry of Glasses, 40, 184–192.

MANUSCRIPT RECEIVED AUGUST 17, 2005
MANUSCRIPT ACCEPTED DECEMBER 30, 2005
MANUSCRIPT HANDLED BY MICHAEL FECHTELKORD